Friction **10**(9): 1405–1423 (2022)
https://doi.org/10.1007/s40544-021-0550-0
ISSN 2223-7690
CN 10-1237/TH
RESEARCH ARTICLE

Ionic liquids as boundary additives in water-based and PAO lubricants

Wahyu WIJANARKO[1,2,*], **Hamid KHANMOHAMMADI**[1], **Nuria ESPALLARGAS**[1,*]

[1] *Norwegian Tribology Center, Department of Mechanical and Industrial Engineering, Norwegian University of Science and Technology (NTNU), Trondheim 7491, Norway*

[2] *Department of Mechanical Engineering, Sepuluh Nopember Institute of Technology (ITS), Surabaya 6011, Indonesia*

Received: 11 March 2021 / Revised: 29 April 2021 / Accepted: 23 August 2021

Abstract: Ionic liquids have been widely discussed as potential lubricants, however, their properties make them also very good potential candidates as lubricant additives (e.g., friction modifiers and anti-wear). In this work, the tribological study of two ionic liquids (tributylmethylphosphonium dimethylphosphate (PP), and 1-butyl-1-methylpyrrolidinium tris(pentafluoroethyl)trifluorophosphate (BMP)) as lubricant additives has been performed on stainless steel (AISI 316L) exposed to polar (water-glycol) and non-polar (polyalphaolefin) based lubricants under boundary lubricating conditions. The performance of these ionic liquids as lubricant additives has been compared to a classical organic friction modifier (dodecanoic acid (C12)). The water–glycol lubricant formulated with the two ionic liquids showed friction values higher than the same base lubricant formulated with dodecanoic acid, however, opposite results were observed for polyalphaolefin (PAO). A detailed surface chemical analysis using X-ray photoelectron spectroscopy (XPS) revealed differences in the passive/tribofilm thickness and chemical composition of the stainless steel surface tested in all lubricants. In the case of the polar lubricant additivated with ionic liquids, the tribochemical reaction accompanied by a tribocorrosion process led to the formation of an unstable passive/tribofilm resulting in high friction and wear. However, in the absence of tribocorrosion process (polyalphaolefin base lubricant), the tribochemical reaction led to the formation of a stable passive/tribofilm resulting in low friction and wear. A detailed surface and subsurface investigation of the microstructure using scanning electron microscopy equipped with a focused ion beam (SEM-FIB) showed that high wear rates resulted in thicker recrystallization region under the wear track surface. Among all lubricant additives tested in this work, BMP in non-polar lubricant media showed the best tribological performance.

Keywords: water lubricant; polyalphaolefin (PAO); ionic liquids; tribochemistry; tribocorrosion; tribofilm

1 Introduction

In this modern era, energy efficiency has become a significant issue in automotive and industrial sectors worldwide. In system components consisting of moving parts, wear and friction play a significant role in the energy consumption. A recent study shows that 23% of the world's total energy consumption was lost in tribological contacts to overcome friction (20%) and to repair the worn parts due to wear or wear-related failures (3%) [1]. Lubrication is needed in moving parts to provide low-friction and wear-protective boundary films to protect surfaces. Lubricants consists of about 70%–99% base oil and 30%–1% chemical additives depending on the application and use of the lubricant. Base oils have two main sources, biological (animal or vegetable sources) and non-biological (mineral or synthetic oils produced by the

* Corresponding authors: Wahyu WIJANARKO, E-mail: wahyu.wijanarko@ntnu.no, wijanarko@me.its.ac.id; Nuria ESPALLARGAS, E-mail: nuria.espallargas@ntnu.no

distillation and cracking process of crude oil) leading to a broad variety of hydrocarbons that can be polar and non-polar. For some specific applications where fire safety is the main requirement, water-based lubricants are also formulated (i.e., typically ca. 1:1 mixture of water and glycols or any other polar hydrocarbon that helps increasing viscosity). The primary function of the base oil is to lubricate and act as a carrier of additives. Additives are chemical compounds that improve the performance of base oils and are meant for enhancing an already existing property (viscosity, pour point, oxidation resistance, etc.) or to add a new property (cleaning/suspending ability, antiwear performance, corrosion control, friction control, etc.). Each additive or group of additives have a function in different or several lubricating regimes (i.e., boundary, mixed, and hydrodynamic regimes). Friction modifiers and anti-wear additives are most critical in the boundary/mixed lubricating conditions and are the focus of this work due to their relevance for future applications in low and ultra-low viscosity lubricants used in, for example, electric vehicles [2].

Commonly used friction modifiers are carboxylic acids which have a polar head and a non-polar hydrocarbon tail. They are commonly known as organic friction modifiers (OFMs). They have been used since the 1920s and due to their amphiphilic molecular structure, the OFMs can be dissolved in polar and non-polar media [3]. The polar head tends to adsorb on metal surfaces while the non-polar tail stretches out to the lubricant base preventing contact between adjacent sliding surfaces thus providing low friction. There are two main parameters limiting the functionality of carboxylic acids, i.e., high temperature and high pressure [4]. When the mechanical conditions in a tribological system become severe (very high pressure in the boundary lubricating regime), the friction modifier on the moving surface tends to desorb. In this extreme boundary lubricating condition, anti-wear additives are then required to preserve the integrity of the surfaces in contact. A well-known anti-wear additive is zinc dialkyldithiophosphate (ZDDP), which was developed in the 1940s as an antioxidant, but its ability to reduce wear was soon discovered [3]. The ability of ZDDP to overcome wear lies on its capability to form a protective film on the metal surface through tribochemical reactions [5]. However, the degradation products of ZDDP pose environmental risks thus its use needs to be reduced to meet the Euro 5 and Euro 6 standards [6, 7]. Therefore, current trends in industry to maintain low friction and wear protection in systems working in boundary lubricating conditions (e.g., electric vehicles using low and ultra-low viscosity lubricants) are pushing the need to find new friction and anti-wear additives with a greener perspective as well, for example, ionic liquids.

Ionic liquids (ILs) are organic salts, containing a positive (cation) and a negative (anion) part, that are liquid at low temperature (usually <100 °C). Ionic liquids are considered as "green" substances due to their extremely low volatility (not emitting hazardous volatile compounds) [8, 9]. But they offer other benefits as well, such as low melting points (liquid at room temperature), chemical and thermal stability (high-temperature operation), non-flammability, high ionic conductivity, high heat capacity, high thermal conductivity (facilitating the removal of excessive heat), and high polarity (highly surface active and adsorbing) [10–12]. Their chemical and physical properties can be tuned by changing the anion and cation composition to obtain task-specific ILs structures. This flexibility makes ILs ideal candidates for lubricants for extreme conditions, such as high shear and high loads, extreme temperatures, and even ultra-high vacuum [13, 14]. In addition, some research works performed on ILs as lubricant additives have proven that ILs have excellent friction-reduction and anti-wear properties [13, 15–17].

The mechanisms by which ILs are potential good candidates as lubricant additives are still not clear in literature and this can be due to the vast amount of chemistries available, making it difficult to find a unique distinctive trend. Two main lubricating mechanisms for ILs are proposed/found in literature: (1) ILs form an adsorbed layer on the metal surface, and (2) ILs form a protective layer (tribofilm) on the metal surface by a tribochemical process [18]. For the first lubricating mechanism, the anions of ILs are attracted by the positively charged metal surface during the rubbing action, subsequently, cations are attracted by anions. Depending on the attraction force between the ions, a monolayer or multilayer structure of anions-cations can be formed originating from the

metal surface towards the bulk lubricant [19–21]. This structure has low shear strength properties thus reduces the friction between the two sliding surfaces [22]. For the second mechanism, ILs between two mating surfaces will be broken down or decomposed due to the localized high temperature and high pressure. The highly active IL anions will eventually react with the metal surface during the rubbing action. A protective tribofilm will be formed as a product of this tribochemical reaction which will eventually increase the wear resistance [23–26].

Since the possibilities for ILs as lubricant additives are many and the trend of low viscosity and environmentally friendly lubricants is increasing, this research work was initiated with the aim to study ILs as potential green additives in two low viscosity lubricant media (one polar and one non-polar). The non-polar lubricant media was a low viscosity and low conductivity polyalphaolefin (PAO). The polar lubricant media chosen was a water–glycol mixture due to its clear compatibility with the environment, but it was also chosen because of its high electrical conductivity with the aim of studying the effect of conductivity in the performance of ILs as lubricant additives. More precisely, the effect of electrical conductivity and the corrosion performance of the ILs were assessed in this work. In this respect, a hybrid tribocorrosion-tribochemical mechanism has been proposed. The tribological performance of the two ILs has been compared with a well-known OFM, dodecanoic acid (C12). The tribological material chosen for this study has been an austenitic stainless steel (AISI 316L) due to its good corrosion resistance. This metal alloy also allows to study the ionic reactivity of ILs towards the properties of the passive/tribofilm. The tribological performance of the different additives is discussed based on a detailed XPS analysis inside and outside the wear tracks, and a microstructural analysis of the wear track subsurface cross-section.

2 Experimental procedure

2.1 Materials

In this work, two ionic liquids were used as lubricant additives in polar and non-polar media. As a reference, a commonly used organic friction modifier (OFM) was chosen. The ionic liquids (ILs) were the following: tributylmethylphosphonium dimethylphosphate (PP) (97% purity and a molar mass of 342.40 g·mol^{-1}) purchased from Fluorochem, and 1-butyl-1-methylpyrrolidinium tris(pentafluoroethyl) trifluorophosphate (BMP) (≥98%, 587.27 g·mol^{-1}) purchased from Sigma-Aldrich. The OFM was a carboxylic acid (dodecanoic acid, abbreviated C12) (≥99%, 200.32 g·mol^{-1}) purchased from Sigma-Aldrich. The chemical structures of all the additives used in this work are presented in Fig. 1. The additives were dissolved in two different media: (1) a polar media consisting of a mixture of water and dipropylene glycol (WG), and (2) a non-polar media consisting of a polyalphaolefin with an aliphatic hydrocarbon chain of 10 carbons (PAO). Dipropylene glycol (≥99%, 134.18 g·mol^{-1}) was purchased from Acros Organics, and the polyalphaolefin was obtained from Chevron Phillips Chemical. All chemicals in these experiments were used as received without further purification. The mixture of the base lubricant with the additives

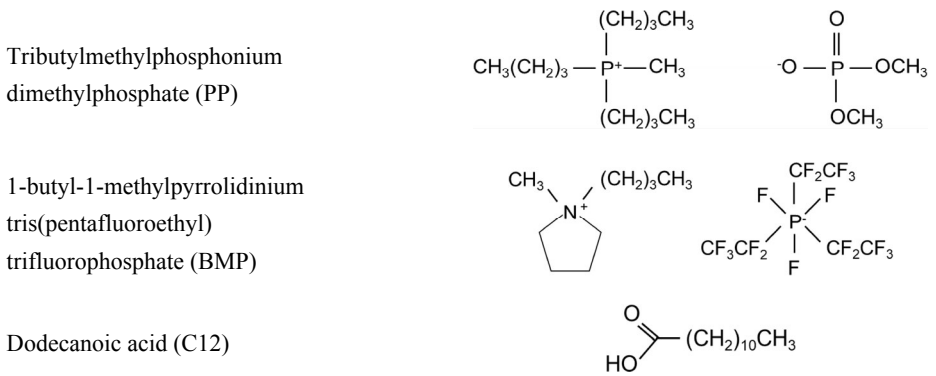

Fig. 1 Molecular structures of the ionic liquids and dodecanoic acid.

was made using a magnetic stirrer for 4 hours at 50 °C and 70 °C for polar and non-polar media, respectively. The additive concentrations used for the tribological studies were 1 wt% and 0.1 wt% for ILs and a carboxylic acid, respectively. In a previous study performed in our research group, the optimal concentration for C12 in the same base lubricants was found to be 0.1 wt% [27]. Therefore, for the present work, 0.1 wt% of C12 was chosen as a reference. In an independent study, we have tested the ILs in both base lubricants at different concentrations (0.25, 0.5, 1, 2, and 4 wt%). In that study, it was found that for the water-based lubricant, the ILs were fully soluble at all concentrations and friction was stable at concentrations equal and above 1 wt%. For the case of PAO, the solubility of ILs varied depending on the IL type. For PP, it was at the same level as in water-glycol and BMP was not fully soluble at any concentration due to its high electronegativity. Therefore, a concentration of 1 wt% was chosen for the ILs in both base lubricants.

Stainless steel 316L samples were cut from a 30 mm diameter stainless steel bar purchased from Smith Stål (Trondheim, Norway) to create disks of 5 mm thickness for tribological testing. The disks were ground using SiC paper and polished using diamond paste to obtain a surface finish of Ra = 0.090 ± 0.003 μm. The roughness was measured using a Mitutoyo SJ-301 surface roughness stylus profilometer. The average surface roughness (Ra) in 0°, 90°, 180°, and 270° directions was chosen to describe the roughness. After grinding and polishing, disks were ultrasonically cleaned in a 1:1 mixture of ethanol and distilled water for 5 minutes. Subsequently, disks were rinsed with ethanol and dried with hot air before testing.

2.2 Testing and characterization methods

Rheometer (Haake Mars Rotational Rheometer with a CC27 cylinder measuring system, with the built-in Peltier element) was used to measure the dynamic viscosity 23 °C in humid air. Each measurement was performed by increasing the shear rate from 0.01 to 500 s^{-1} with a ramp time of 180 seconds, then held at a constant shear rate of 500 s^{-1} for 30 seconds, and continued by decreasing the shear rate from 500 to 0.01 s^{-1} with a ramp time of 180 seconds. The dynamic viscosity was reported from the average value of 30 measurements taken during the lubricant was held at a constant shear rate of 500 s^{-1}. The dynamic viscosity values are presented in Table 1. There is a significant difference in dynamic viscosity between WG and PAO. However, adding the additives does not significantly change the dynamic viscosity of any of these two base lubricants.

A turbidity meter (Hanna Instruments HI-88713) was used to examine the stability of the lubricant mixture at room temperature. Turbidity measures the appearance of lubricants by the degree of light that has been scattered by the insoluble additives in the lubricant. With increasing in scattered light, the turbidity will be higher; i.e., higher Formazin Nephelometric Units (FNU). The lubricants were put on a magnetic stirrer for 2 hours prior to the test. The reported FNU was measured by calculating the average value of 12 measurements taken from 2 hours test. Turbidity values are shown in Table 1. WG and PAO base lubricants have stable turbidity numbers of 0.25 and 0.1 FNU, respectively, being transparent and without phase separation. Lubricants with additives show similar turbidity number and stable values as their base lubricant, except for PAO-BMP, which increases turbidity number to 0.84 FNU and shows a cloudy appearance, indicating that it is not fully soluble in PAO.

The conductivity of the lubricants was measured using a conductivity meter (Hanna Instruments HI-2300). The pH of the lubricant was measured using a pH meter from Radiometer analytical (PHM220 Lab

Table 1 Physical and electrical properties of all lubricants.

Lubricants	Dynamic viscosity (mPa·s)	Turbidity (FNU)	Conductivity (μS/cm)*	pH
WG	13.99	0.25	2.5	7.3
WG–C12	13.53	0.25	4.3	4.7
WG–PP	13.76	0.13	211.2	3.4
WG–BMP	14.02	0.17	109.3	7.0
PAO	81.29	0.12	n.d.	n.d.
PAO–C12	83.13	0.21	n.d.	n.d.
PAO–PP	87.27	0.12	n.d.	n.d.
PAO–BMP	85.23	0.84	n.d.	n.d.

* For comparison, the conductivity of tap water is ca. 500 μS/cm and for seawater is ca. 5,000 μS/cm.

pH Meter). These measurements only apply to polar lubricants (WG) with and without additives, since the non-polar lubricant (PAO) has non-detectable conductivity or pH due to the lack of sufficient ionic species. Conductivity and pH results are presented in Table 1. C12 does not significantly increase the conductivity of the base lubricant compared to ionic liquids. Ionic liquids increase the conductivity in 2 orders of magnitude. Among the ILs, PP presents the highest conductivity compared to BMP. Adding C12 and PP to WG changes the pH towards acidic values, with PP having the greatest effect. However, BMP does not change the pH value of the base lubricant.

A unidirectional ball-on-disk tribometer (Phoenix tribology) was used to evaluate the tribological performance of the lubricant under boundary conditions. An alumina (fused ceramic) ball with a diameter of 6 mm, purchased from Precision Ball and Gauge Co., Ltd., was pushed against the stainless steel 316L disk with a free-weight load of 20 N, which corresponds to a maximum Hertzian contact pressure of 1.96 GPa. The rotation of the disk was set to 40 rpm with a track diameter of 10 mm, which gives a sliding speed of 2.09 cm/s. The calculated lambda (λ) value, according to the EHL Hamrock-Dowson formula, is 0.016 and 0.088 for WG and PAO, respectively, and therefore the boundary lubrication condition is met for both lubricants. The addition of an additive to the base lubricant slightly changes the viscosity value, but the lambda value still meets the boundary lubrication condition. Testing WG and PAO with C12 additive served as the reference. All lubricants were tested at room temperature. The distance of the tribological test was set to 300 meters (4 hours duration). Three experiments were performed to verify the repeatability of the results for each condition.

The wear volume was quantified with Alicona Infinite Focus optical 3D microscope and MountainsMap surface imaging, analysis, and metrology software. The wear volume was measured from four locations of the wear track for each sample and the average value was then calculated. Subsequently, from three samples for each condition, Archard's equation was used to calculate the average specific wear rate (SWR) [28]:

$$\mathrm{SWR} = \frac{V}{N \cdot S}$$

where SWR is a specific wear rate ($mm^3/(N \cdot m)$), V is the volume loss (mm^3), N is the normal load (N), and S is the sliding distance (m).

The wear track morphology was observed using FEI Quanta FEG 650 Scanning Electron Microscopy (SEM) and the wear track cross sections were prepared and observed with FEI Helios Nanolab DualBeam focused ion beam (FIB) and SEM. Gallium liquid metal ion source was used for deposition, milling, and polishing. Prior to milling, a platinum layer of 24 μm × 7 μm × 5 μm was deposited on the wear track's surface to protect the surface from damage during the ion milling process. In FIB images, this platinum layer will be seen as a black layer on top of the surface. Milling was carried out to the depth of 15 μm using the gallium source with a voltage of 30 kV and a current of 21 nA in the right, front, and left of the protective platinum layer. The cross section cleaning procedure was done in two steps using a current of 6.5 nA and 0.92 nA with a voltage of 30 kV. The lower current was applied to minimize artifacts such as curtaining and to get maximum grain contrast. Grain contrast of wear track cross section was revealed in SEM mode using through-lens-detector (TLD).

X-ray photoelectron spectroscopy (XPS) was used to perform detail chemical analysis of the inside and outside of the wear tracks by a Kratos Axis Ultra DLD machine using monochromatic Al Kα source (10 mA, 10 kV). The sample analysis chamber was set to a vacuum of 9×10^{-9} Torr during the acquisition. A survey scan was performed to collect the elemental map of the surface using pass energy of 160 eV and step size of 1 eV. From the elemental map, several elements were selected for further detailed high resolution scan, i.e., nickel (Ni), iron (Fe), chromium (Cr), molybdenum (Mo), carbon (C), oxygen (O), phosphorus (P), and fluorine (F), using pass energy of 20 eV and step size of 0.1 eV. Depth profile chemical analysis was performed to study the tribofilm. Sputtering was performed using Argon ion gun with a pressure of 4.4×10^{-7} Torr, an energy of 4 kV, and a raster size of 2.5 × 2.5 mm. The selected sputtering times were 0, 5, 15, 35, 85, 185, 685, and 1685 seconds. CasaXPS software was used for evaluation and quantification. Detail curve-fitting parameters for different compounds used for evaluation and quantification are shown in Table 2.

Table 2 Detail curve-fitting parameters of compounds detected outside and inside the wear track of the stainless steel after tribo-testing.

Signal	Binding energy (± 0.1 eV)	FWHM (± 0.1 eV)	Line shape	Assignment	Reference
Ni 2p	855.9	1.8	GL(30)	$Ni(OH)_2$	[29, 30]
	853.7	1.8	GL(30)	NiO	
	852.7	0.9	GL(30)	Ni $2p_{3/2}$	
Fe 2p	714.4	2.9	GL(30)	FeF_3	[16, 31, 32]
	712.8	2.9	GL(30)	Fe^{3+}	
	712.6	2.9	GL(30)	$FePO_4$	
	711.0	2.9	GL(30)	Fe_3O_4	
	709.5	2.9	GL(30)	FeO	
	706.7	0.9	LF(0.8,2,20,0)	Fe $2p_{3/2}$	
F 1s	684.9	1.6	GL(30)	F^-	[16, 33]
Cr 2p	578.7	1.5	GL(30)	CrO_3	[31, 32]
	577.3	1.5	GL(30)	$Cr(OH)_3$	
	576.1	1.5	GL(30)	Cr_2O_3	
	573.9	1.2	LF(0.8,2,8,0)	Cr $2p_{3/2}$	
O 1s	533.3	1.8	GL(30)	O–C, O=C	[32, 34]
	531.4	1.8	GL(30)	O–H	
	530.1	1.1	GL(30)	O–M	
Mo 3d	235.6	1.3	GL(30)	$Mo^{6+(ox)}$ $3d_{3/2}$	[35]
	232.4	1.3	GL(30)	$Mo^{6+(ox)}$ $3d_{5/2}$	
	234.2	1.6	GL(30)	$Mo^{4+(hyd)}$ $3d_{3/2}$	
	231.0	1.6	GL(30)	$Mo^{4+(hyd)}$ $3d_{5/2}$	
	232.3	0.9	GL(30)	$Mo^{4+(ox)}$ $3d_{3/2}$	
	229.1	0.9	GL(30)	$Mo^{4+(ox)}$ $3d_{5/2}$	
	230.6	0.7	LF(1.1,2.3,2,0)	Mo $3d_{3/2}$	
	227.6	0.7	LF(1.1,2.3,2,0)	Mo $3d_{5/2}$	
C 1s	289.3	1.3	GL(30)	O–C=O	[36–38]
	288.2	1.3	GL(30)	C=O	
	286.5	1.3	GL(30)	C–OH, C–O–C	
	285.4	1.0	GL(30)	C–N	
	285.0	1.0	GL(30)	C–C	
P 2p	133.6	1.6	GL(30)	(PO_4^{3-})	[38, 39]

3 Results

3.1 Tribological testing

Sliding tests were performed on stainless steel under the boundary lubricating regime conditions to study the influence of ionic liquids as boundary lubricant additives in polar and non-polar base lubricants. Figures 2(a) and 2(b) show the friction evolution over the whole distance for the base lubricants, base lubricants with ionic liquids (PP and BMP), and base lubricants with reference additive (C12) in polar (WG) and non-polar (PAO) media, respectively. Friction evolution of WG and PAO base lubricants alone are characterized by a long running-in distance with high friction, reaching steady friction values of 0.145

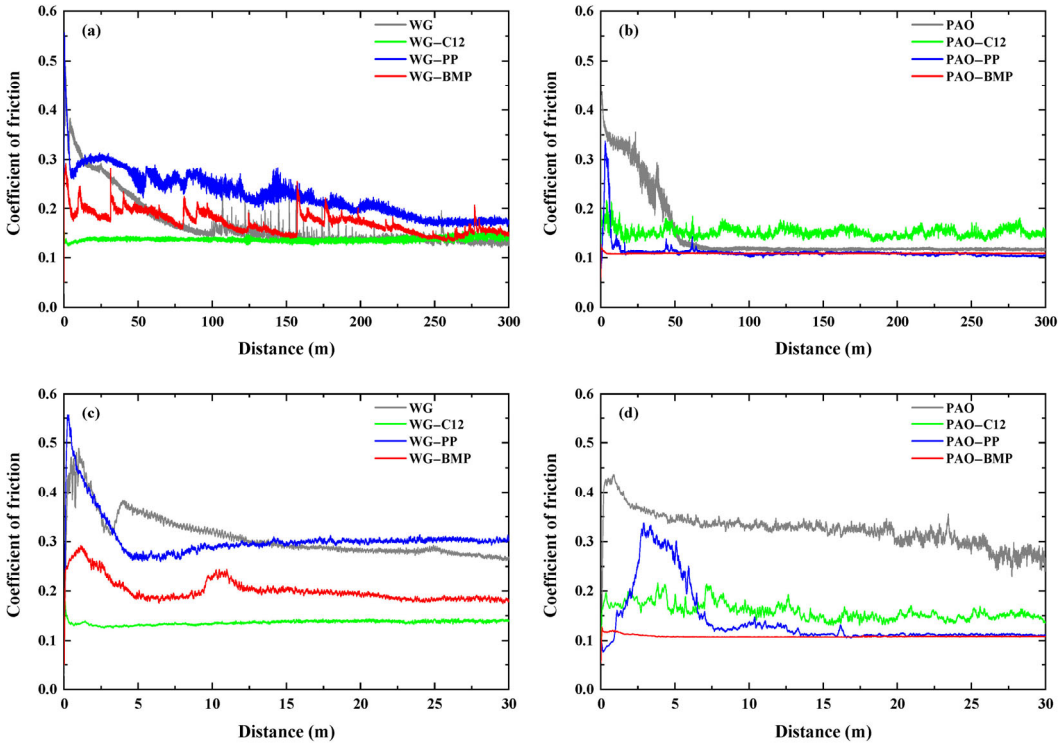

Fig. 2 The friction evolution at room temperature for (a) WG with and without additive, (b) PAO with and without additive, (c) the running-in period for WG, and (d) running-in period for PAO. Only one friction evolution graph is shown for each test due to the excellent repeatability of the results.

and 0.112 for WG and PAO after ca. 100 and 50 m sliding distance, respectively. Adding C12 to WG suppresses the running-in sliding distance (Fig. 2(c)) and keeps friction similar to the WG base lubricant alone after running-in. C12 in PAO shortens the running-in sliding distance to 10 m (Fig. 2(d)) but increases the friction to 0.15 with respect to the base lubricant alone. The addition of 1 wt% of ILs to WG significantly affects the friction evolution of this base lubricant. There is a sudden drop in friction at the start of the test (5 m sliding distance, Fig. 2(c)) and then the friction continues decreasing with time with some abrupt increments in some places until a sliding distance of 200 m (Fig. 2(a)). The ionic liquids in PAO reduce the running-in sliding distance (Fig. 2(d)), and friction after running-in is almost similar to the PAO base lubricant alone. Among the two ILs, BMP is the best in reducing the running-in period in PAO and it gives the lowest friction evolution in WG.

The specific wear rate (SWR) was calculated from the volume loss measured by 3D optical microscope, and the results are shown in Fig. 3. The SWR value of the base lubricants (WG and PAO) alone are 7.83×10^{-6} mm^3/(N·m) and 1.68×10^{-5} mm^3/(N·m), respectively. The carboxylic acid increases the SWR in approximately 5 and 4 times as compared to the base lubricants alone. PP in WG doubles the SWR, whereas BMP gives a similar SWR value as the WG base lubricant alone. The presence of ILs in PAO decreases the SWR with respect to PAO alone. The highest reduction occurs with BMP by approximately 82% compared to PAO alone.

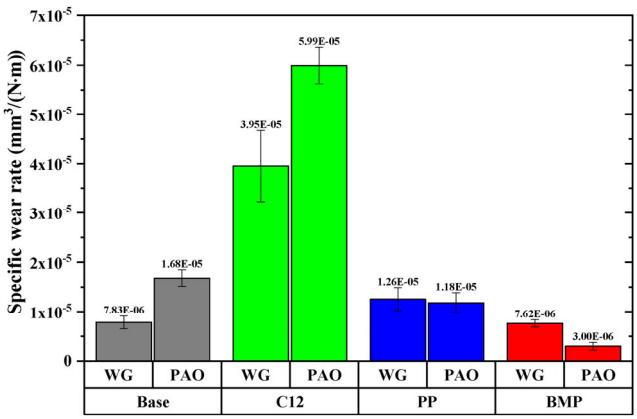

Fig. 3 The influence of carboxylic acid and ionic liquids on the wear rate of stainless steel.

3.2 Wear track morphology

Figure 4 shows the SEM images of the wear tracks on stainless steel disk lubricated by polar and non-polar base lubricant with and without additives. The wear track morphology for stainless steel lubricated by WG base lubricant alone shows a smooth surface with signs of wear and pits in several locations. These pits indicate cracks that propagate through the surface leading to material detachment. The material lubricated by PAO base lubricant alone, shows a smooth wear track surface with signs of abrasive wear and plastic deformation. When using carboxylic acid as additive, very fine wear scars with no signs of plastic deformation are observed in WG–C12. On the other hand, severe plastic deformation is observed on the surface lubricated by PAO with C12 additive.

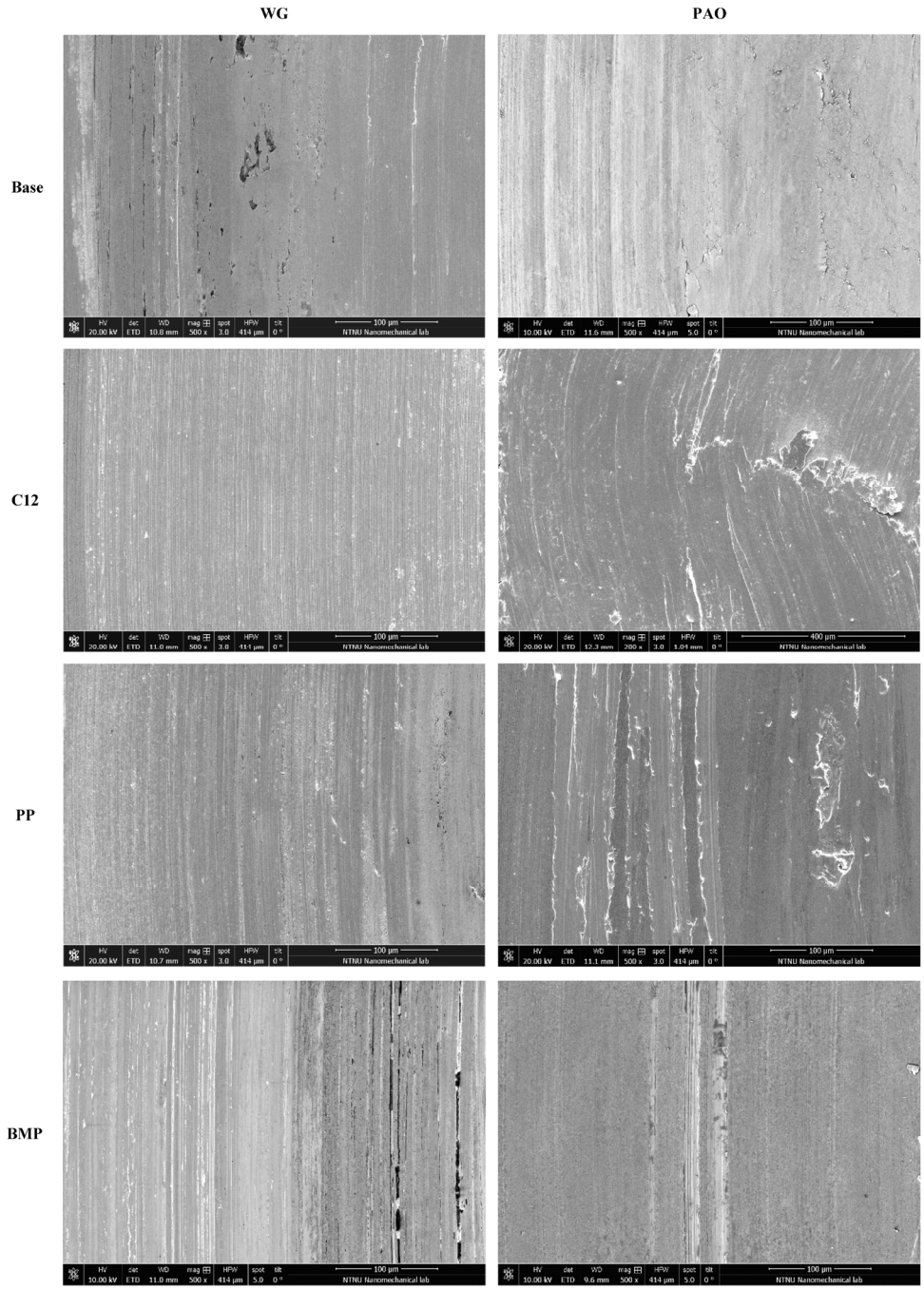

Fig. 4 SEM images of the wear tracks on stainless steel disk tested in different lubricants at room temperature. Pictures were taken with 500x magnification except for PAO–C12 with 200× magnification.

The wear tracks of stainless steel lubricated by WG–PP and WG–BMP show similar wear morphology, i.e., abrasive wear with little signs of plastic deformation with WG–BMP having the smoothest surface. Stainless steel lubricated by PAO–PP shows plowing with signs of plastic deformation and some delaminated areas. On the other hand, different wear mechanism is found for stainless steel lubricated by PAO–BMP. In this case, a smoother surface and abrasive grooves with no signs of plastic deformation can be found. From the wear track images, BMP seems to give a better effect on wear morphology than PP both in polar and non-polar base lubricant, which is in agreement with the friction evolution and SWR results.

The cross section subsurface microstructures prepared by FIB are shown in Fig. 5. The images were taken at the center of the wear track and perpendicular to the sliding direction. For all samples, the subsurface

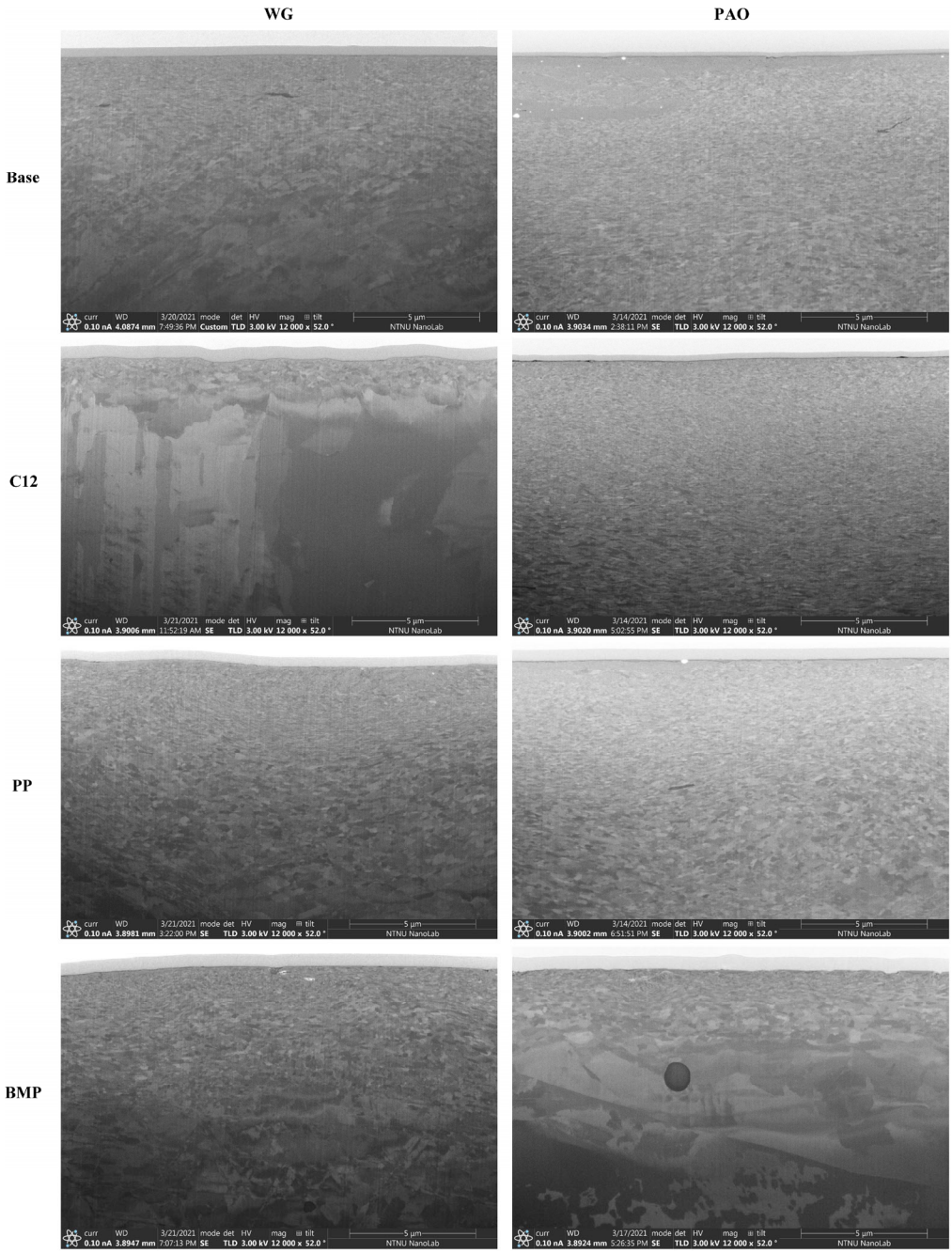

Fig. 5 FIB cross-sections of the wear tracks of stainless steel tested with different lubricants at room temperature.

microstructure of stainless steel exhibited different extents of grain refinement and plastic deformation. When testing with the base lubricant alone, finer grain recrystallization deeper along the cross section was observed for stainless steel lubricated by PAO compared to WG. Adding C12 to the base lubricant resulted in very different subsurface grain features. C12 in WG gives a thinner subsurface recrystallization area, whereas C12 in PAO resulted in a thicker subsurface recrystallization area with finer grains. This is in line with the higher friction evolution of PAO–C12 (Fig. 2), which gives higher shear forces resulting in higher shear strain at the surface and subsurface areas.

Comparing the subsurface microstructures of stainless steel lubricated by WG–PP and WG–BMP, similar grain refinement or recrystallization has occurred. On the other hand, different subsurface microstructures were observed for stainless steel lubricated by PAO–PP and PAO–BMP. In the case of PAO–PP, very fine grain structure close to the surface in nanometer size can be observed. Contrary, thinner recrystallization area was observed for stainless steel lubricated by PAO–BMP, indicating lower shear strain occurring in the subsurface region. This result is in agreement with lower friction and wear during the test.

3.3 Passive film thickness and surface chemical composition

Surface chemical composition inside and outside the wear tracks was studied by X-ray photoelectron spectroscopy (XPS) for base lubricant with additives and untested 316L stainless steel served as a reference. Argon sputtering was applied to perform depth profiling in order to study the passive/tribofilm thickness and its chemical composition. For each sputtering time, the percentage of atomic concentration was calculated based on peak areas obtained from the high resolution XPS spectra of each element (graphs are not shown in this paper). For all test conditions, a decrease in oxygen concentration and an increase in metallic concentration as sputtering time increased were observed, getting close to the chemical composition of the bulk stainless steel. The oxygen peak versus sputtering time was used to calculate the passive film thickness. Passive film thickness can be defined by sputtering time when the oxygen peak concentration reaches 50% of the maximum value [40]. To calibrate the sputtering rate with passive film thickness, tantalum oxide (Ta_2O_5) with known thickness was sputtered with the same procedure. The obtained sputter rate was 2 nm per minute for Ta_2O_5. Table 3 shows the passive film thickness inside and outside of the wear track calculated with respect to Ta_2O_5. The passive film thickness of untested 316L was 1.87 nm, which is in agreement with the results obtained from other authors [41–43]. Thicker passive film thickness outside the wear track was observed for all stainless steel tested with WG with respect to the reference sample, however, in the case of PAO thicker passive film was only observed using C12 as additive. Comparing inside and outside of the wear track (i.e., ratio inside/outside), thicker passive film thickness was observed for all lubricant formulations, except for PAO–C12.

A detailed XPS analysis was made to study the passive film composition from the high resolution XPS spectra inside and outside of the wear tracks, and on the reference sample. Curve-fitting parameters in Table 2 were used in CasaXPS software to quantify the relative concentration of the compounds. A detailed procedure for calculating the relative concentration between compounds can be found elsewhere [44]. Figure 6 shows the subsurface relative atomic concentration of the passive film component from high resolution XPS spectra of chromium (Cr) and iron (Fe) inside and outside of the wear tracks and on the reference sample. Cr peaks consist of Cr^0, Cr_2O_3, $Cr(OH)_3$, and CrO_3, and Fe peaks consist of Fe^0, FeO, Fe_3O_4, Fe^{3+} (i.e., FeOOH and $Fe(OH)_3$), $FePO_4$, and FeF_3. It can be seen that the passive film formed on the stainless steel surface when tested in lubricants

Table 3 Passive film thickness inside and outside of the wear track.

		Passive film thickness (nm)		
Untested SS316L		1.87		
Base lubricant	Position	Additive		
		C12	PP	BMP
WG	Outside	3.30	3.67	2.43
	Inside	3.47	8.50	13.50
	Ratio inside/outside	1.05	2.32	5.55
PAO	Outside	2.97	1.83	1.87
	Inside	2.60	11.63	10.17
	Ratio inside/outside	0.88	6.36	5.44

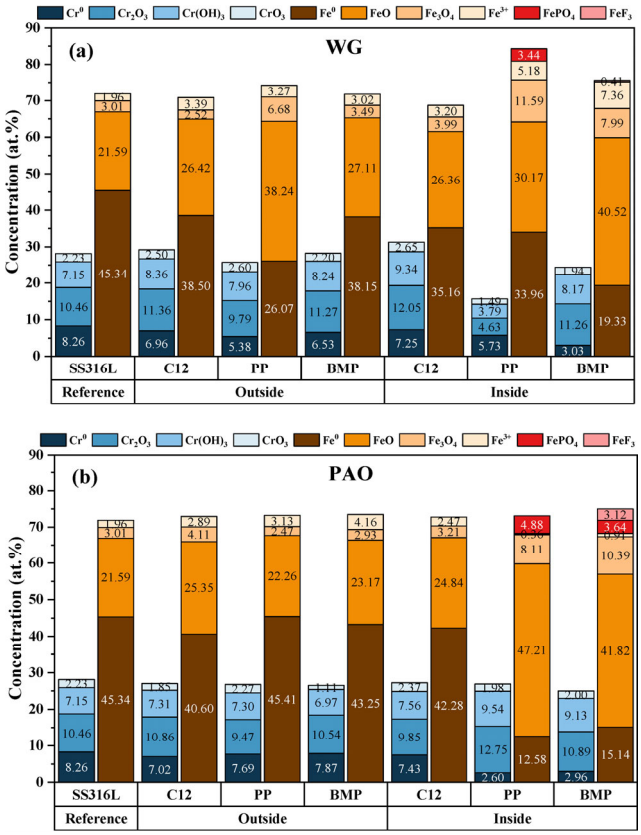

Fig. 6 Relative atomic concentration of Cr and Fe species inside and outside the wear track of the stainless steel tested with different lubricant formulations, (a) in WG and (b) in PAO (taken from sputtering time 35 seconds).

with C12 additive inside the wear track consists of oxides and hydroxides only. However, phosphate and fluoride were found in the passive films inside the wear track of the stainless steel material tested with lubricant containing ionic liquid additives indicating a tribochemical reaction during the rubbing action. Moreover, iron hydroxides were suppressed in the presence of phosphate and fluoride for non-polar lubricant.

4 Discussion

4.1 Effect of the base fluid polarity and tribocorrosion on friction

The reference lubricant additive used in this work was a classical organic friction modifier (OFM), dodecanoic acid (C12). When this additive was added to the polar (WG) and non-polar (PAO) lubricant, different friction values and evolution with time were obtained. C12 in WG fully suppressed the running-in period and it shortened the running-in period from 50 to 10 meters in PAO as compared to the base lubricant alone. The lowest and more stable friction evolution was obtained in WG, which can be attributed to the surface coverage of this additive to the metal surface. Before rubbing starts, C12 instantaneously adsorbs onto the metal surface. Indeed, it was found that more adsorption to the metal surface for WG–C12 (19.35 at%) compared to PAO–C12 (15.39 at%) when considering the relative concentration of O–C=O and C=O bonds found by XPS (Fig. 7). Most studies of carboxylic acids used as lubricant additives are performed in non-polar base lubricants (mineral or synthetic oils). For these types of base lubricants, two adsorption mechanisms of carboxylic acids to metal surfaces have been proposed in literature: (1) carboxylic acid molecules and surface oxide or hydroxide form a hydrogen bond, or (2) formation of metal carboxylates [45–47]. However, when polar lubricants (mostly water-based) are used, the adsorption of carboxylic

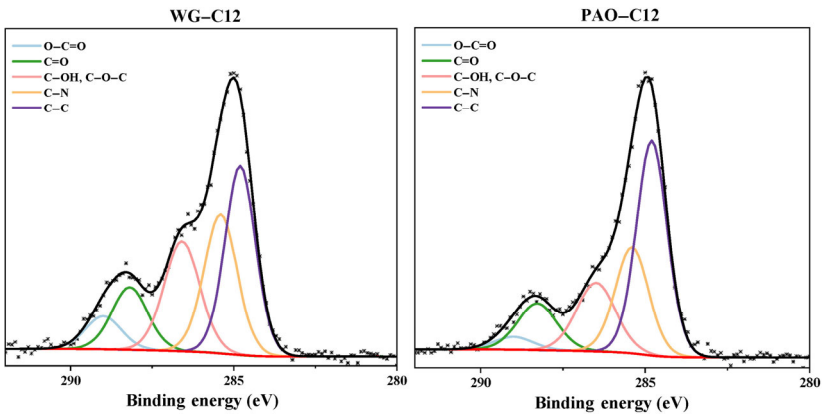

Fig. 7 C 1s spectra on the stainless steel surface outside the wear track lubricated by WG–C12 and PAO–C12.

acid to the metal surface is different due to the deprotonation of the carboxylic head in water. In a previous study, it was found that the carboxylic acid C12 in water-based lubricant has a tendency to form a multilayer brush structure, efficiently separating the two mating sliding surfaces thus reducing friction in a more efficient way than in non-polar lubricant [27]. In addition, this mechanism depends on the concentration of the additive (for WG) and on the length of the carboxylic chain (for PAO). In WG, when the carboxylic acid concentration is higher than the critical micelle concentration (CMC), the deprotonated carboxylic acids form micelles separating the sliding surfaces even more efficiently, and in non-polar media (PAO) the longer the carboxylic chain the more efficient the surface separation is [27]. Therefore, in this work the very short chain of C12 was not sufficient in PAO to keep an efficient separation of the sliding surfaces and friction was higher than in WG where a multilayer of additive kept a very efficient separation of the surfaces decreasing friction. These differences in friction are evident from the FIB cross sections of the wear tracks, where the recrystallized region in WG–C12 is thinner than the one in PAO–C12 (Fig. 5).

Due to the sliding action, the adsorbed carboxylic acid reacts with the metal to form a tribofilm [32, 47]. The passive film thickness inside the wear track was analyzed by XPS and values of 3.47 and 2.60 nm were found for WG–C12 and PAO–C12, respectively (Table 3). The passive films inside the wear tracks are tribofilms mostly composed of oxides and hydroxides (Fig. 6) since the stainless steel material is oxidized on the surface (i.e., passive film) and the carboxylic acid mostly contains C, H, and O. A further analysis of the XPS results has been performed to calculate the oxide and hydroxide to metal ratios (Cr and Fe) inside and outside the wear tracks (Fig. 8). Comparing these ratios inside the wear track, it can be seen that more oxide and hydroxide are present for WG–C12 than for PAO–C12. This is in agreement with more additive adsorption on the surface and a thicker passive/tribofilm, thus leading to a more efficient friction reduction for WG–C12 than for PAO–C12.

Interestingly, the ILs show different friction results than the reference additive (C12), being lowest for PAO–ILs and highest for WG–ILs. Clearly, the passive/tribofilms inside the wear track are thicker when the base lubricants are additivated with ILs (Table 3) and this effect is also seen outside the wear track for WG. These differences in passive/tribofilm thickness are accompanied by different surface chemistry as compared to C12, i.e., higher oxide and hydroxide to metal ratio is found together with P and F (Figs. 6 and 8). In addition, the Fe oxide to metal ratio significantly increases inside the wear track for all ILs, and outside the wear track for PP only. Worth noticing is that the Fe oxide to metal ratio remained constant both inside and outside the wear track for C12. The presence of F^- and PO_4^{3-} compounds (Figs. 6 and 9) make the passive film thicker, being ILs the triggers for a tribochemical reaction that promotes the formation of Cr and Fe ions that further react with oxygen, phosphorous and fluorine (Figs. 8 and 9). This surface tribochemical reaction has a clear detrimental effect in WG by creating fluctuations in the friction evolution, whereas in PAO it creates a

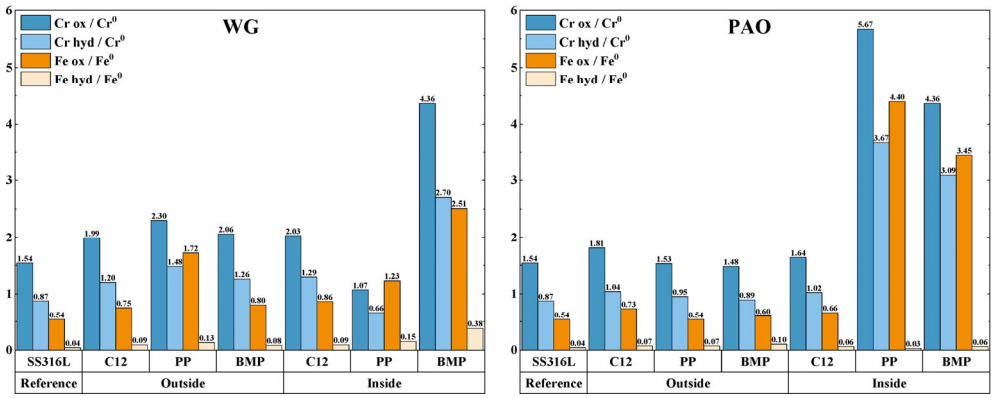

Fig. 8 The intensity ratio of oxide and hydroxide with respect to the metallic part for Cr and Fe for all lubricants inside and outside the wear track.

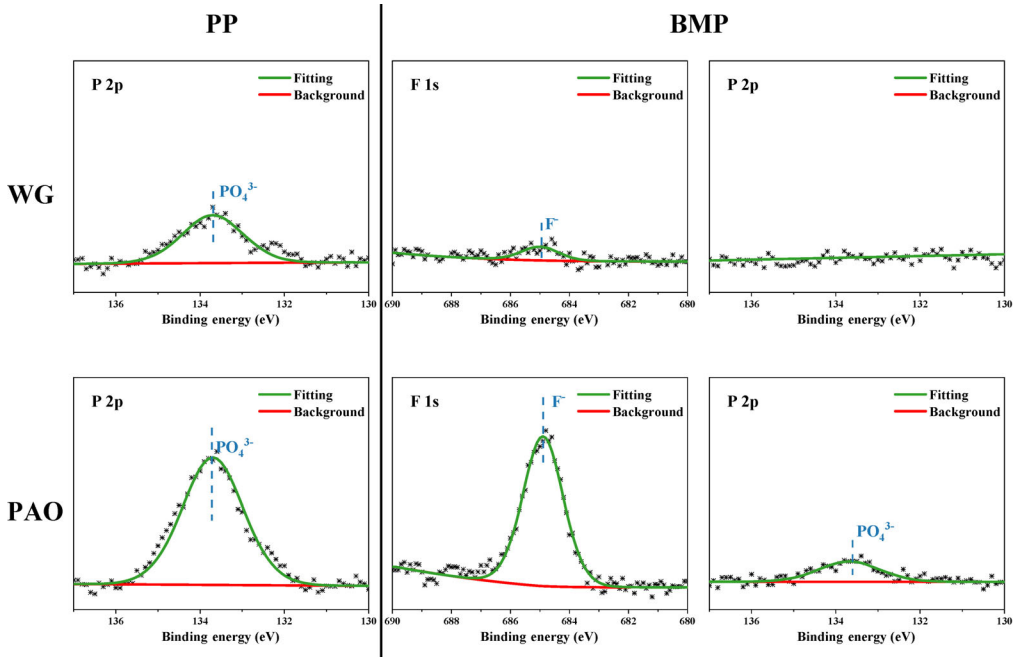

Fig. 9 F 1s and P 2p spectra inside the wear track of the stainless steel lubricated by WG–PP, WG–BMP, PAO–PP, and PAO–BMP (taken from sputtering time 35 seconds).

thick and durable tribofilm that stabilizes friction (Fig. 1). The fluctuations in WG are to be understood as depassivation–repassivation events due to the high electrical conductivity of the media. Therefore, friction evolution in WG is mainly controlled by tribocorrosion [48], whereas in PAO it is controlled by the tribochemical reaction that creates a thick and durable tribofilm. The lowest friction was obtained for PAO–BMP and WG–BMP for each base lubricant and their respective tribofilms contained mostly FeF_3 (Figs. 6 and 9). Therefore, F contributes to the tribochemical reaction enhancing the tribofilm formation [49]. However, this process is more efficient in PAO since, due to the lack of electrical conductivity, it does not compete with tribocorrosion. Thus, more FeF_3 and some traces of $FePO_4$ are found in PAO–BMP, whereas in WG–BMP only traces of FeF_3 are found (Fig. 9).

A special case is PP, which creates a tribofilm of mostly $FePO_4$ in both WG and PAO (Fig. 9). Indeed, big differences in the Fe and Cr oxides both inside and outside the wear tracks are found for PP. An increase in the amount of Fe and Cr oxide outside the wear track and a significant decrease inside the wear track are found in WG with respect to PAO. In addition, PP leads to the lowest inside/outside passive film thickness ratio for WG among all ILs mixtures tested (Table 3). This is in agreement with its highest conductivity and lowest pH in WG (Table 1). Due to the high conductivity, fast repassivation kinetics for PP are to be expected in the wear track during the sliding action in water. However, the very low pH leads to a high (active) metal dissolution resulting in lower oxide and hydroxide to metal ratio compared to outside the wear track (Fig. 8). BMP has an electrical conductivity in the same order of magnitude as PP, however due to the neutral pH of the solution, the dissolution of Cr and Fe oxide was slower in WG (Fig. 8). The higher electrical conductivity and the lowest pH of PP resulted in a thinner tribofilm and therefore in higher friction for WG–PP than WG–BMP. Since PAO is a non-conductive medium, tribocorrosion does not take place and therefore the friction evolution only depends on the tribochemical reaction of the additives with the metal surface. Indeed, more $FePO_4$ and FeF_3 are always found in the wear tracks of PAO (Fig. 6).

4.2 Effect of tribocorrosion and pH on wear

Wear rates in the different lubricants varied significantly, being the highest wear rate for the lubricants additivated with C12 (Fig. 3). A detailed investigation of the metal subsurface microstructure in the wear track shows a high recrystallization region for all

testing conditions, but with varying depth (Fig. 5), which is a well-known phenomenon in tribology [50–52]. This subsurface investigation revealed thicker recrystallization region when wear rate was higher for same additive in different media. This effect is clear comparing WG–C12 with PAO–C12 and WG–BMP with PAO–BMP, however, the causes for each pair are different. The adsorption of C12 on the stainless steel surface depended on the polarity of the media leading to a thinner tribofilm in the case of PAO–C12 resulting in thicker recrystallization region and higher wear. For PAO–BMP, a thick and durable tribofilm was formed on the metal surface resulting in limited subsurface recrystallization and the lowest material removal of all studied base and additive pairs. In the case of PP, the wear rate has been mostly controlled by electrical conductivity and pH (i.e., tribocorrosion and metal dissolution).

Further analysis of the wear track cross sections revealed the formation of ridges adjacent to the wear groove as shown in Figs. 10(a) and 10(b). The ridges are to be understood as material displacement to the sides of the wear track indicating signs of plastic deformation. The measured areas of the wear groove (A_{groove}) and ridges (A_{ridges}) are presented in Fig. 10(c) and Fig. 10(d) for WG and PAO with and without additive, respectively, along with the degree of material loss (β). The degree of material loss is defined as the ratio of material loss to the volume of the wear track groove and it has been calculated by using the following equation [53]:

$$\beta = \frac{A_{groove} - A_{ridges}}{A_{groove}} \times 100\%$$

β becomes zero when the material loss is due to plastic deformation only ($A_{groove} = A_{ridges}$), and β becomes unity when the material loss is due to abrasive wear ($A_{ridges} = 0$). Indeed, when the WG lubricants are additivated with ILs, they suffer more abrasive wear characterized by higher β values compared to PAO–ILs (Fig. 10). This effect is clearer for PP and it is aggravated by the low pH values (i.e., PP shows the largest values of A_{groove}). This is in agreement with the fact that the tribocorrosion mechanism in WG has competed with the tribofilm formation resulting in higher material removal rates. The corrosiveness of polar media on metals is mainly dependent on oxygen

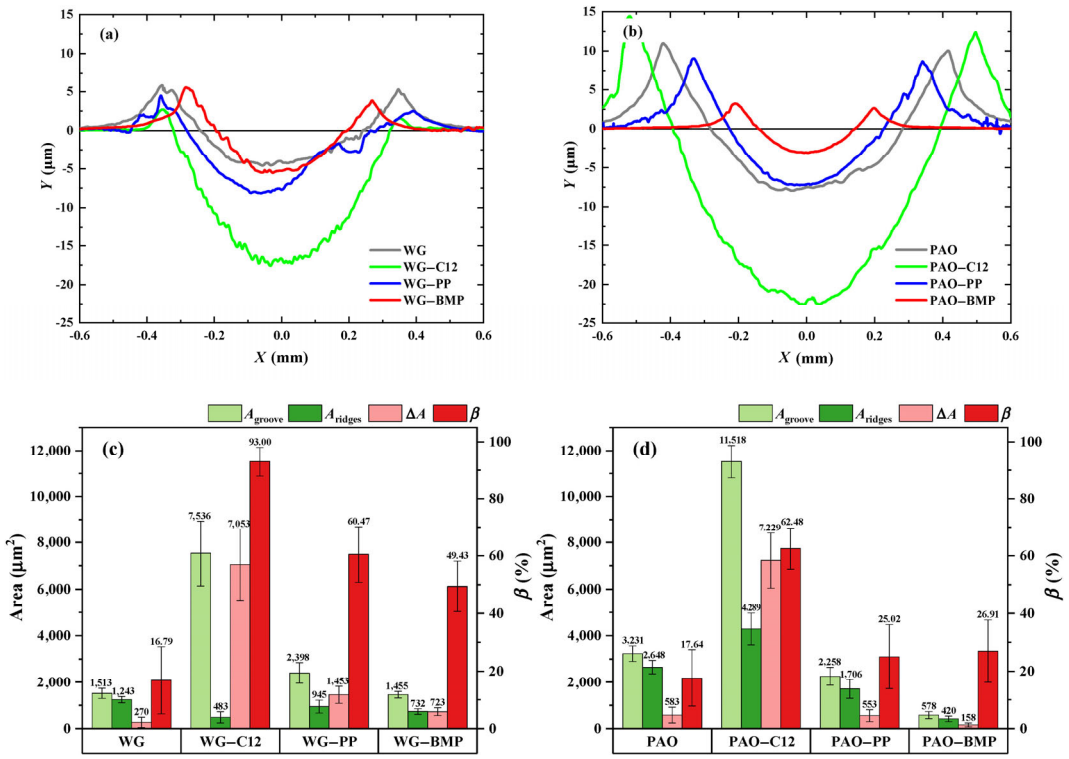

Fig. 10 Wear cross section profile for (a) WG with and without additive, (b) PAO with and without additive, (c) calculated area of (a), and (d) calculated area of (b).

content, electrical conductivity, temperature, and pH. Stainless steel 316L protects itself from corrosion by creating a passive film (chromium oxide) on the surface due to the high content in Cr. During the tribotest, when rubbing starts, this passive film is removed by the mechanical action of the counterpart and the pristine metal alloy (depassivated wear track) will be then exposed to the lubricant. If the lubricant contains oxygen and is electrically conductive, the passive film will reform almost instantaneously (i.e., repassivation process). This process (tribocorrosion) will continue in a cyclic manner until the mechanical action is stopped, leading to an increase in the wear rate of the material [48].

A very interesting case is C12, which has the lowest conductivity in WG and therefore it should be expected to suffer of more plastic deformation. The very low conductivity of WG–C12 slowed down the repassivation kinetics (absence of tribocorrosion) and produced a thin passive film that resulted in higher wear than otherwise expected. In addition, the acidic pH that this additive brings to the WG lubricant (4.7) has played the most important role in the wear process. This very low pH accelerates the active dissolution of the metal in the contact area and therefore very high values of A_{groove} (abrasive wear) and little signs of plastic deformation are found for WG–C12. Indeed, the opposite was found in similar tests performed previously at higher pH (ca. 8) for C12 in WG, where lower wear rates and thicker passive films were found [32, 54].

The passive/tribofilm thickness has also played an important role in the wear performance of the additives. Indeed, this work shows that ILs can function as anti-wear additives in both WG and PAO, whereas C12 can only function as friction modifier. For the ILs, the passive/tribofilm thickness inside the wear track was very thick (Table 3). Comparing WG and PAO additivated with ILs, a competition effect between electrical conductivity and pH is observed. The higher conductivity enhanced the repassivation kinetics for both ILs resulting in a thicker tribofilm as compared to C12. But on the other hand, the low pH of PP increased the metal dissolution thinning the tribofilm for WG–PP, whereas PP in PAO–PP did not have any detrimental effect on the wear rate or on the tribofilm thickness. The polarity of the base lubricant has played a crucial role for PP, dissociating in water (i.e., increasing the electrical conductivity and decreasing pH) and remaining intact in PAO (i.e., enhancing a tribochemical reaction with the metal). In addition, the presence of $FePO_4$ and FeF_3 compounds inside the wear tracks (Figs. 6 and 8) contributed to keeping a very low wear rate due to the creation of thicker and more durable films on the metal surface. This effect is more evident in PAO since the absence of electrical conductivity (i.e., very low ion mobility) mostly promotes the adsorption of the additive on the surface and the subsequent tribochemical reaction with the metal.

Figure 11 summarizes the frictional and wear mechanisms of PP and BMP in polar (water-based) and non-polar (PAO) lubricants as studied in this work. Worth noticing is the tribocorrosion process that occurred in the polar lubricant and the tribochemical process that occurred in the non-polar lubricant. The interplay of these two effects was driven by the polarity of the medium, the electrical conductivity, and the pH leading to different friction and wear results.

5 Conclusions

The effect of ionic liquids on friction and wear of 316L stainless steel tested in both polar and non-polar lubricants has been investigated and compared with carboxylic acid (C12) as reference additive. The following conclusions can be drawn from this work:

- The carboxylic acid (C12) in the polar lubricant showed lower friction than that in the non-polar lubricant due to higher adsorption on the metal surface and thicker passive film. However, the lower conductivity of the lubricants additivated with C12 resulted in thinner passive film compared to lubricants additivated with ionic liquids thus leading to high wear (i.e., the main role of C12 main is as a friction modifier).
- Ionic liquids contribute to a higher electrical conductivity and therefore tribocorrosion played the most important role in the frictional evolution in WG. This effect was suppressed in PAO and therefore friction values depended mostly on the adsorption and tribochemical reaction of the additives with the metal surface.
- Ionic liquids form a thicker passive/tribofilm that results in lower wear for the non-polar base

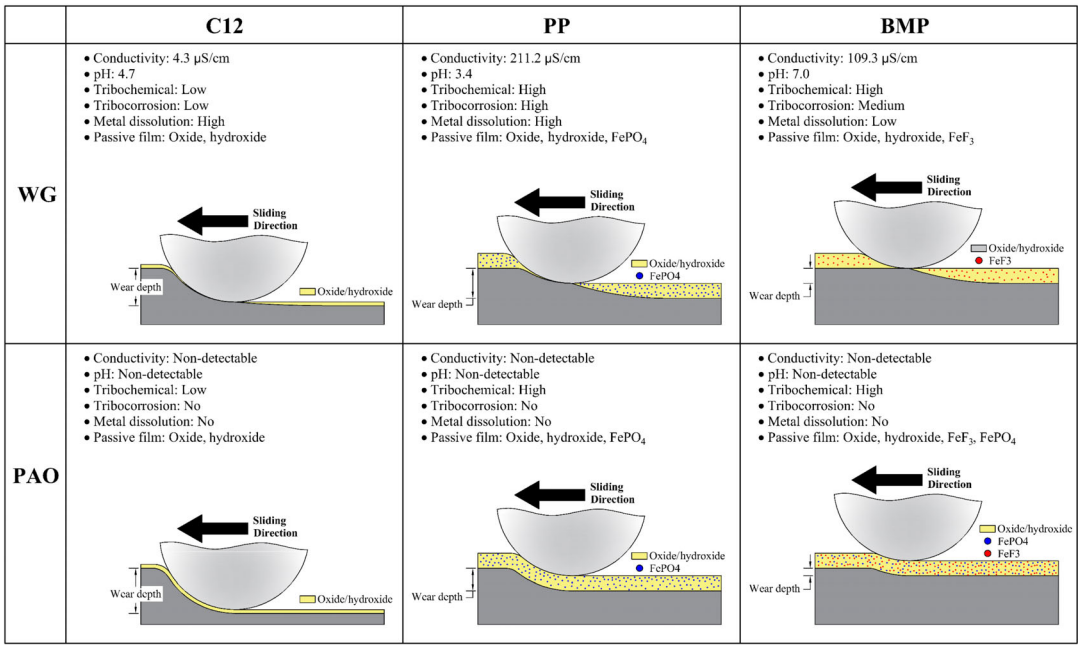

Fig. 11 Schematic illustration of the wear mechanism of SS316L in different lubricating conditions.

lubricant. In addition, the passive/tribofilm created on the surface contains $FePO_4$ and FeF_3, which contributes both to thickening the tribofilm and to keeping low friction and wear.

- In the polar lubricant, the pH played an important role, the lower pH dissolves the passive film resulting in thinner passive/tribofilm thus leading to higher friction and wear. This effect was suppressed in the non-polar lubricant.
- Among all additives tested, BMP shows the best wear and frictional performance in both polar and non-polar lubricants. In the case of the polar lubricant, the neutral pH resulted in less metal dissolution and the intermediate electrical conductivity resulted in a mild tribocorrosion process keeping FeF_3 in the passive/tribofilm thus decreasing wear and friction. In the case of the non-polar lubricant, tribocorrosion is absent and the tribochemical reaction leads to the formation of a thick P and F containing tribofilm that decreases friction and wear.

Acknowledgements

The authors would like to acknowledge the financial support from Indonesia Endowment Fund for Education (LPDP), M-ERA.NET GreenCOAT project with Project Number 4153, and the Norwegian Micro- and Nano-fabrication facility, NorFab, for providing the characterization facilities.

References

[1] Holmberg K, Erdemir A. Influence of tribology on global energy consumption, costs and emissions. *Friction* **5**(3): 263–284 (2017)

[2] Farfan-Cabrera L I. Tribology of electric vehicles: A review of critical components, current state and future improvement trends. *Tribol Int* **138**: 473–486 (2019)

[3] Spikes H. Friction modifier additives. *Tribol Lett* **60**(1): 5 (2015)

[4] Guegan J, Southby M, Spikes H. Friction modifier additives, synergies and antagonisms. *Tribol Lett* **67**(3): 83 (2019)

[5] Barnes A M, Bartle K D, Thibon V R A. A review of zinc dialkyldithiophosphates (ZDDPS): Characterisation and role in the lubricating oil. *Tribol Int* **34**(6): 389–395 (2001)

[6] Spikes H. The history and mechanisms of ZDDP. *Tribol Lett* **17**(3): 469–489 (2004)

[7] Commission Regulation (EU) No. 136/2014 of 11 February 2014. https://eur-lex.europa.eu/eli/reg/2014/136/oj.

[8] Earle M J, Seddon K R. Ionic liquids. Green solvents for the future. *Pure Appl Chem* **72**(7): 1391–1398 (2000)

[9] Zhao H. Innovative applications of ionic liquids as "green" engineering liquids. *Chem Eng Commun* **193**(12): 1660–1677 (2006)

[10] Seddon K R. Ionic liquids for clean technology. *J Chem Tech Biotechnol* **68**(4): 351–356 (1997)

[11] Welton T. Room-temperature ionic liquids. Solvents for synthesis and catalysis. *Chem Rev* **99**(8): 2071–2084 (1999)

[12] Wasserscheid P, Welton T. *Ionic Liquids in Synthesis*. Weinheim (Germany): Wiley-VCH Verlag GmbH & Co. KGaA, 2002.

[13] Bermúdez M D, Jiménez A E, Sanes J, Carrión F J. Ionic liquids as advanced lubricant fluids. *Molecules* **14**(8): 2888–2908 (2009)

[14] Palacio M, Bhushan B. A review of ionic liquids for green molecular lubrication in nanotechnology. *Tribol Lett* **40**(2): 247–268 (2010)

[15] Somers A E, Khemchandani B, Howlett P C, Sun J Z, MacFarlane D R, Forsyth M. Ionic liquids as antiwear additives in base oils: Influence of structure on miscibility and antiwear performance for steel on aluminum. *ACS Appl Mater Interfaces* **5**(22): 11544–11553 (2013)

[16] Viesca J L, García A, Battez A H, González R, Monge R, Fernández-González A, Hadfield M. FAP^- anion ionic liquids used in the lubrication of a steel-steel contact. *Tribol Lett* **52**(3): 431–437 (2013)

[17] Song Z H, Liang Y M, Fan M J, Zhou F, Liu W M. Ionic liquids from amino acids: Fully green fluid lubricants for various surface contacts. *RSC Adv* **4**(37): 19396–19402 (2014)

[18] Xiao H P. Ionic liquid lubricants: Basics and applications. *Tribol Trans* **60**(1): 20–30 (2017)

[19] Atkin R, Abedin S Z E, Hayes R, Gasparotto L H S, Borisenko N, Endres F. AFM and STM studies on the surface interaction of [BMP]TFSA and [EMIm]TFSA ionic liquids with Au(111). *J Phys Chem C* **113**(30): 13266–13272 (2009)

[20] Perkin S, Albrecht T, Klein J. Layering and shear properties of an ionic liquid, 1-ethyl-3-methylimidazolium ethylsulfate, confined to nano-films between mica surfaces. *Phys Chem Chem Phys* **12**(6): 1243–1247 (2010)

[21] Foulston R, Gangopadhyay S, Chiutu C, Moriarty P, Jones R G. Mono- and multi-layer adsorption of an ionic liquid on Au(110). *Phys Chem Chem Phys* **14**(17): 6054–6066 (2012)

[22] Zhou F, Liang Y M, Liu W M. Ionic liquid lubricants: Designed chemistry for engineering applications. *Chem Soc Rev* **38**(9): 2590–2599 (2009)

[23] Qu J, Bansal D G, Yu B, Howe J Y, Luo H M, Dai S, Li H Q, Blau P J, Bunting B G, Mordukhovich G, et al. Antiwear performance and mechanism of an oil-miscible ionic liquid as a lubricant additive. *ACS Appl Mater Interfaces* **4**(2): 997–1002 (2012)

[24] Zhou Y, Dyck J, Graham T W, Luo H M, Leonard D N, Qu J. Ionic liquids composed of phosphonium cations and organophosphate, carboxylate, and sulfonate anions as lubricant antiwear additives. *Langmuir* **30**(44): 13301–13311 (2014)

[25] Barnhill W C, Qu J, Luo H M, Meyer III H M, Ma C, Chi M F, Papke B L. Phosphonium-organophosphate ionic liquids as lubricant additives: Effects of cation structure on physicochemical and tribological characteristics. *ACS Appl Mater Interfaces* **6**(24): 22585–22593 (2014)

[26] González R, Bartolomé M, Blanco D, Viesca J L, Fernández-González A, Battez A H. Effectiveness of phosphonium cation-based ionic liquids as lubricant additive. *Tribol Int* **98**: 82–93 (2016)

[27] Bernat S, Armada S, Espallargas N. Friction mechanisms by carboxylic acids in aqueous lubricants. *Tribol Lett* **66**(3): 83 (2018)

[28] Archard J F. Contact and rubbing of flat surfaces. *J Appl Phys* **24**(8): 981–988 (1953)

[29] Casella I G, Guascito M R, Sannazzaro M G. Voltammetric and XPS investigations of nickel hydroxide electrochemically dispersed on gold surface electrodes. *J Electroanal Chem* **462**(2): 202–210 (1999)

[30] Lei Y, Jiang J L, Bi T T, Du J F, Pang X J. Tribological behavior of *in situ* fabricated graphene-nickel matrix composites. *RSC Adv* **8**(39): 22113–22121 (2018)

[31] Fredriksson W, Malmgren S, Gustafsson T, Gorgoi M, Edström K. Full depth profile of passive films on 316L stainless steel based on high resolution HAXPES in combination with ARXPS. *Appl Surf Sci* **258**(15): 5790–5797 (2012)

[32] Zavieh A H, Espallargas N. The effect of friction modifiers on tribocorrosion and tribocorrosion-fatigue of austenitic stainless steel. *Tribol Int* **111**: 138–147 (2017)

[33] Yu B, Zhou F, Pang C J, Wang B, Liang Y M, Liu W M. Tribological evaluation of α, $\acute{\omega}$-diimidazoliumalkylene hexafluorophosphate ionic liquid and benzotriazole as additive. *Tribol Int* **41**(8): 797–801 (2008)

[34] Long Y, De Barros Bouchet M I, Lubrecht T, Onodera T, Martin J M. Superlubricity of glycerol by self-sustained chemical polishing. *Sci Rep* **9**(1): 6286 (2019)

[35] Marcus P, Bussell M E. XPS study of the passive films formed on nitrogen-implanted austenitic stainless steels. *Appl Surf Sci* **59**(1): 7–21 (1992)

[36] Ding Y F, Zhang F, Xu J C, Miao Y Q, Yang Y Z, Liu X G, Xu B S. Synthesis of short-chain passivated carbon quantum dots as the light emitting layer towards electroluminescence. *RSC Adv* **7**(46): 28754–28762 (2017)

[37] Li H P, Zhu S W, Zhang M, Wu P W, Pang J Y, Zhu W S, Jiang W, Li H M. Tuning the chemical hardness of boron nitride nanosheets by doping carbon for enhanced adsorption capacity. *ACS Omega* **2**(9): 5385–5394 (2017)

[38] Urtis L A, Arcifa A, Zhang P, Du J X, Fantauzzi M, Rauber D, Hempelmann R, Kraus T, Rossi A, Spencer N D. Influence of water on tribolayer growth when lubricating steel with a fluorinated phosphonium dicyanamide ionic liquid. *Lubricants* **7**(3): 27 (2019)

[39] Rokosz K, Hryniewicz T, Simon F, Rzadkiewicz S. Usporedne XPS analize sastojaka pasivnih slojeva nastalih na Duplex 2205 SS poslije standardnog elektropoliranja i elektropoliranja strujom velike gustoće. *The Vjesn* **23**(3): 731–735 (2016)

[40] Kirchheim R, Heine B, Fischmeister H, Hofmann S, Knote H, Stolz U. The passivity of iron-chromium alloys. *Corros Sci* **29**(7): 899–917 (1989)

[41] Wang Z C, Di-Franco F, Seyeux A, Zanna S, Maurice V, Marcus P. Passivation-induced physicochemical alterations of the native surface oxide film on 316L austenitic stainless steel. *J Electrochem Soc* **166**(11): C3376–C3388 (2019)

[42] Wang Z C, Paschalidou E M, Seyeux A, Zanna S, Maurice V, Marcus P. Mechanisms of Cr and Mo enrichments in the passive oxide film on 316L austenitic stainless steel. *Front Mater* **6**: 232 (2019)

[43] Detriche S, Vivegnis S, Vanhumbeeck J F, Felten A, Louette P, Renner F U, Delhalle J, Mekhalif Z. XPS fast depth profile of the native oxide layers on AISI 304, 316 and 430 commercial stainless steels and their evolution with time. *J Electron Spectrosc Relat Phenom* **243**: 146970 (2020)

[44] Mischler S, Mathieu H J, Landolt D. The investigation of passive films on iron—Chromium alloys by AES and XPS. *Surf Interface Anal* **12**(7): 429 (1988)

[45] Sahoo R R, Biswas S K. Frictional response of fatty acids on steel. *J Colloid Interf Sci* **333**: 707–718 (2009)

[46] Lin M M, Kim D K. In situ thermolysis of magnetic nanoparticles using non-hydrated iron oleate complex. *J Nanopart Res* **14**(2): 688 (2012)

[47] Simič R, Kalin M. Adsorption mechanisms for fatty acids on DLC and steel studied by AFM and tribological experiments. *Appl Surf Sci* **283**: 460–470 (2013)

[48] Munoz A I, Espallargas N, Mischler S. *Tribocorrosion*. Cham (Switzerland): Springer International Publishing, 2020.

[49] Hu E Z, Dearn K, Yang B X, Song R H, Xu Y F, Hu X G. Tribofilm formation and characterization of lubricating oils with biofuel soot and inorganic fluorides. *Tribol Int* **107**: 163–172 (2017)

[50] Rice S L, Nowotny H, Wayne S F. Formation of subsurface zones in impact wear. *ASLE Trans* **24**(2): 264–268 (1981)

[51] Büscher R, Fischer A. The pathways of dynamic recrystallization in all-metal hip joints. *Wear* **259**(7–12): 887–897 (2005)

[52] Perret J, Boehm-Courjault E, Cantoni M, Mischler S, Beaudouin A, Chitty W, Vernot J P. EBSD, SEM and FIB characterisation of subsurface deformation during tribocorrosion of stainless steel in sulphuric acid. *Wear* **269**(5–6): 383–393 (2010)

[53] Bruce R W. *Handbook of Lubrication and Tribology*, *Volume II*: *Theory and Design*. 2nd ed. New York (USA): CRC Press, 2012.

[54] Bernat S, Armada S, Espallargas N. Effect of contamination on the friction and wear of carboxylic acids in aqueous lubricants. *Tribol Lett* **66**(4): 158 (2018)

Wahyu WIJANARKO. He received his bachelor degree in mechanical engineering in 2005 from Sepuluh Nopember Institute of Technology, Surabaya, Indonesia. Then, he received his master degree in materials science in 2010 from University of Aveiro, Portugal. Currently he is a Ph.D. student in Norwegian Tribology Center, Department of Mechanical and Industrial Engineering, Norwegian University of Science and Technology, Trondheim, Norway. His research interests include tribology and lubrication.

Hamid KHANMOHAMMADI. He received his master degree in materials science and engineering in 2011 from University of Tehran, Iran. He received his Ph.D. degree in materials engineering from the same university in 2017, focused on tribocorrosion behaviour of PEO coatings. Currently he is a postdoctoral researcher in Norwegian Tribology Center, Department of Mechanical and Industrial Engineering, Norwegian University of Science and Technology, Trondheim, Norway. His research areas are tribocorrosion, water-based lubricants, and surface interactions in tribology.

Nuria ESPALLARGAS. She is a professor at the Department of Mechanical and Industrial Engineering of the Norwegian University of Science and Technology (NTNU, Norway). She has a M.S. degree in chemistry and a Ph.D. degree in surface engineering from University of Barcelona (Spain). Since 2011 she is the NTNU leader of the Gemini Centre Tribology. She has performed two international research stays at EPFL and ETH (Switzerland) in the fields of tribocorrosion and nano-tribology. Her scientific and research interests are within surface chemistry and engineering, tribology, lubricants, tribocorrosion, and nano-tribology.